Received: 8 June 2022 | Revised: 30 September 2022 | Accepted: 21 October 2022

DOI: 10.1002/jrs.6465

RESEARCH ARTICLE

Journal of RAMAN SPECTROSCOPY WILEY

Density functional theory demonstrates orientation effects in the Raman spectra of hydroxy- and carbonated apatite

Dejan Gemeri[1,2,3] | **Aleksandar Živković**[2] | **Igor Lukačević**[3] | **Hilke Bahmann**[1] | **Helen E. King**[2]

[1]Physical and Theoretical Chemistry, Bergische Universität Wuppertal, Wuppertal, Germany

[2]Department of Earth Sciences, Utrecht University, Utrecht, The Netherlands

[3]Department of Physics, Josip Juraj Strossmayer University of Osijek, Osijek, Croatia

Correspondence
Aleksandar Živković, Department of Earth Sciences, Utrecht University, Princetonlaan 8a, 3584CB Utrecht, The Netherlands.
Email: a.zivkovic@uu.nl

Abstract

Raman spectroscopy is widely used to examine the carbonate content within bone apatite, but Raman spectra are also sensitive to orientation effects between the polarisation of the incoming laser light and the sample orientation. This may lead to discrepancies when using Raman spectroscopy to evaluate the carbonate content as the extent of crystal organisation can change depending on the type of bone, age, and presence of mineralisation disorders in the organism. It is experimentally very challenging to evaluate the effect of orientation using individual bone crystals. Therefore, we have used density functional theory to examine the effect of orientation in apatitic materials. We examined hydroxyapatite and three different types of carbonated apatite: A-type where the carbonate ion substitutes the two OH groups in the unit cell, B-type where co-substitution occurs between carbonate in a phosphate position and Na^{+} for Ca^{2+} to maintain charge balance, and AB-type where carbonate sits in both A-site and B-site. Our simulations show that the OH group in hydroxyapatite has a strong orientation dependence, consistent with previous literature. In addition, the phosphate and carbonate bands of the apatitic structures are predicted to be orientation dependent, where the maximum scattering efficiency occurs in configurations in which the laser polarisation is parallel to the crystallographic axes of the material. The intensity changes of the phosphate and carbonate bands are not consistent upon changing orientations and thus may lead to an underestimation of carbonate contents if insufficient sampling points are used during bone analysis.

KEYWORDS

bone, carbonated apatite, density functional theory, hydroxyapatite, orientation effects

Dejan Gemeri and Aleksandar Živković contributed equally.

1 | INTRODUCTION

Biological apatite found in bone, dentine, and enamel[1] is an inorganic, crystalline calcium phosphate material with an atomic structure similar to that of abiotic hydroxyapatite (OHAp) found in geological materials. However, unlike its abiological counterpart, significant chemical substitutions are found associated with this material, particularly the occlusion of carbonate ions (CO_3^{2-}) either in place of a hydroxyl (A-type) or phosphate (B-type) group.[2] These substitutions dramatically change the physical and chemical properties of the crystals,[3,4] enabling them to have specific functionalities in biological tissues. Due to this, significant amounts of research have been undertaken in the materials and medical science domains as changes in the chemical reactivity of the material can be related to pathological mineralisation, such as in cardiovascular disease, deficient mineralisation,[5] including osteoporosis,[6] and are important for the biocompatibility of bone and teeth implants.[7] Thus, it is of great importance to characterise and gain insight into defective OHAp structures. A key analytical tool for probing chemical changes in bioapatite, that is the go-to method for the materials and medical scientific communities, is vibrational spectroscopy: infrared (IR) and Raman spectroscopies. For example, pristine vibrational bands respond to the chemical environment of the carbonate group incorporated into the structure via the formation of new vibrational bands.[8–10] These methodologies are considered so robust that it has become a standard procedure to obtain the carbonate percentage in biological apatite from the ratio of the carbonate band(s) intensity versus the intensity of the dominant phosphate band. However, there have been reports that the relative intensities of the Raman bands are dependent on the orientation of the crystals with respect to the incoming light source,[11,12] which can be highly variable in materials such as bone and dentine and change with age of the organism[13] or tissue and in the presence of mineralisation disorders.[14]

Raman spectroscopy is increasingly the focus of such research as it has been suggested to be more sensitive to carbonate substitutions[15] and it is relatively easy to examine the effects of orientation using this technique. As a technique, it is particularly interesting for medical research because there is a potential to apply it in vivo,[16–18] unlike many orientation and compositional analytical techniques, for example, 2D X-ray tomography or electron microscopy. Hydroxyapatite and enamel have been measured using a Raman spectrometer under different laser polarisations at selected orientations, and results show that some band intensities have a strong dependence on the sample orientation.[19,20] Similarly, bone samples orientated differently with respect to laser polarisation produce Raman spectra where the intensity of the biological apatite related bands varies.[21] Yet, the reported behaviour of the bands between these studies is inconsistent. Particularly, the effect on the symmetric stretching band of PO_4 (ν_1) is critical because this is the band that is used to normalise intensities between spectra to calculate the carbonate concentration. In large, abiotic hydroxyapatite crystals the intensity of the ν_1 PO_4 band is found to show minimal change with orientation,[20] yet within bone, this effect is significant.[14] In contrast to bone and dentine biological apatite, enamel crystals are typically 100 times larger, have a lower carbonate content, and have higher crystallinity.[22–24] Whether carbonated apatite shows a similar orientational relationship to abiotic hydroxyapatite is unclear from the current studies. To the best of our knowledge, orientation experiments with synthetic carbonated hydroxyapatites have not been reported in the literature, probably due to the logistical difficulties associated with the small size of the crystallites produced. Similarly, mineral components in bone and dentine are too small to evaluate the effect of orientation on individual crystals. Therefore, in this study, we have used density functional theory to determine the effect of laser polarisation and sample orientation on the Raman spectra of carbonated apatites.

2 | METHODS

Density functional theory (DFT) calculations presented in this work were performed using a linear combination of atomic orbitals (LCAO) basis set as implemented in the all-electron code CRYSTAL (2017 release),[25,26] where the atoms were described using basis sets reported in literature (calcium,[27] phosphorus,[28] oxygen,[29] hydrogen,[30] carbon,[31] and sodium[32]). The global hybrid B3LYP exchange-correlation functional[33,34] was used throughout all calculations without further modifications. The geometry of each system under scrutiny was optimised in both atomic coordinates and cell parameters, while the Hessian was updated using the Broyden-Fletcher-Goldfarb-Shanno (BFGS) algorithm.

In CRYSTAL, the convergence of the real-space summation of the Coulomb and exchange contributions to the Hamiltonian matrix is controlled by five overlap criteria. The values used in this study were 10^{-6}, 10^{-6}, 10^{-6}, 10^{-6}, and 10^{-12}. The threshold on the self-consistent (SCF) energy was set to 10^{-7} Ha. For the compounds of interest, the convergence with respect to k-points was

checked. Monkhorst-Pack meshes of 2 × 2 × 4 for bulk hexagonal hydroxyapatite and 2 × 4 × 1 for bulk monoclinic hydroxyapatite were used to sample the first Brillouin zone.[35]

Relative Raman intensities were computed analytically based on coupled-perturbed Hartree-Fock/Kohn-Sham (CPHF/KS) treatments implemented in the code.[36,37] Integrated Raman intensities are normalised so that the most intense peak is set to 1000. The peak width is not explicitly available within this treatment; thus, it was kept constant. The spectra are constructed by using the transverse optical modes and adopting a pseudo-Voigt function with the default VOIGT and DAMPFAC variables of 1.0 (pure Lorentzian functions) and 8.0 (full width at half maximum used for the spectra), respectively. The temperature and laser frequency, taken into account through a prefactor in the expression for the Raman integrated intensity, were set to 295 K and 532 nm to facilitate comparison with available experimental measurements. In CRYSTAL, the Raman spectra are obtained for an oriented single crystal and for a powder polycrystalline sample. Different polarisation components are identified from the components of the polarisability tensor. The standard polarisation notation is used throughout the work; for example, the *xy* polarisation denotes the response of the material in the *x*-direction as a result of an applied incident light source polarised in the *y*-direction. Upon analysing the resulting spectra, the unit cell orientation axis were translated where required to a common reference system (chosen to be the initial pristine hexagonal bulk OHAp one, which corresponds closest to the crystallographic one) for consistent and relevant comparison between the systems under scrutiny. Furthermore, the chosen setup has been shown to reproduce the structure as well as vibrational properties of apatite compounds in good agreement with experimental data.[38–41] Anharmonicity has been taken into account only for the O–H stretching mode.[42,43]

Long range dispersion corrections were included using the semi empirical D3 approach of Grimme et al. with Becke–Johnson damping.[44–46] Graphical drawings were produced using VESTA.[47] The crystal structures and their corresponding lattice directions used throughout this work are shown in Figure 1. Hexagonal OHAp was modelled in a unit cell with $P6_3$ (nr. 173) symmetry, instead of the experimentally noted $P6_3/m$ (nr. 176) space group to avoid the unphysical duplication of each OH group[29]; monoclinic OHAp was modelled in a cell with $P2_1/b$ symmetry (nr. 14), while all the carbonate-bearing models are simulated in a triclinic trivial $P1$ symmetry (nr. 1). Estimations of the intensities related to orientations other than the six calculated (*xx*, *xy*, *xz*, *yy*, *yz*, and *zz*) were found using a locally modified Matlab script (originating from the VASPKIT MAE script[48]) whereby the intensities were linearly interpolated before being plotted in a 3D diagram where notation of the plot axes corresponded to the crystallographic axes.

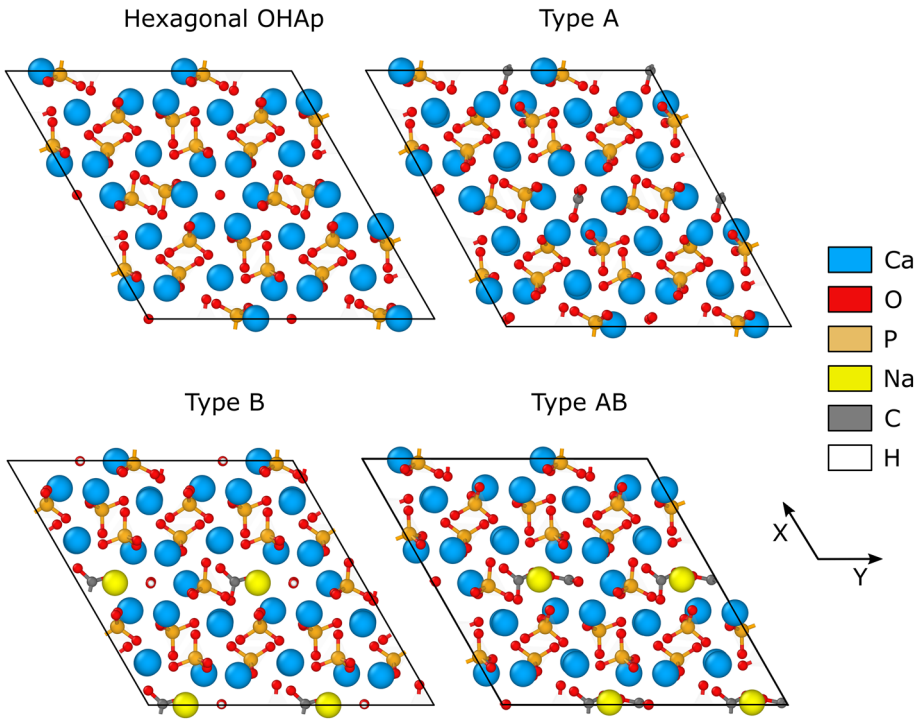

FIGURE 1 Crystal structure of the four distinct unit cells coupled with DFT used to determine the effect of laser polarisation and sample orientation on the Raman spectra of carbonated apatites [Colour figure can be viewed at wileyonlinelibrary.com]

3 | RESULTS AND DISCUSSION

3.1 | Geometrical features

The calculated lattice parameters of pristine as well as carbonated hydroxyapatite are listed in Table S1. The calculated values compare well to experimentally available data as well as earlier theoretical works, which is not surprising as the adopted methodology and simulated geometries have been audited and elaborated upon extensively in available literature.[2,29,41,49–51] It is, however, noted that the inclusion of weak van der Waals (dispersive) forces (via the Grimme's D3 semiempirical approach) yields lattice constants that systematically underestimate the lattice parameters of OHAp when compared to experiments. Further system-dependent tuning of the dispersion parameters would be required to achieve results closer to measured ones, as demonstrated by Civalleri and co-workers,[52] which was not pursued here in order to present a systematic study with consistent parameters across all OHAp systems. The comparison of anharmonic corrections to the OH stretching modes is reported in Table S2. As CRYSTAL only applies anharmonic effects to stretching modes, it is difficult to make full comparison with experimental data for reasons outlined elsewhere.[53]

3.2 | Hydroxyapatite

Calculations of the effect of incoming light polarisation with respect to the crystal structure orientation calculated using DFT demonstrate that all bands in the Raman spectrum display an orientation dependency of their intensity (Figure 2A). Typically, the orientation of the incoming light perpendicular to the major crystal axes results in the lowest band intensities observed. The exception to this was the symmetric bending ν_2 PO_4 band at 474 cm^{-1},

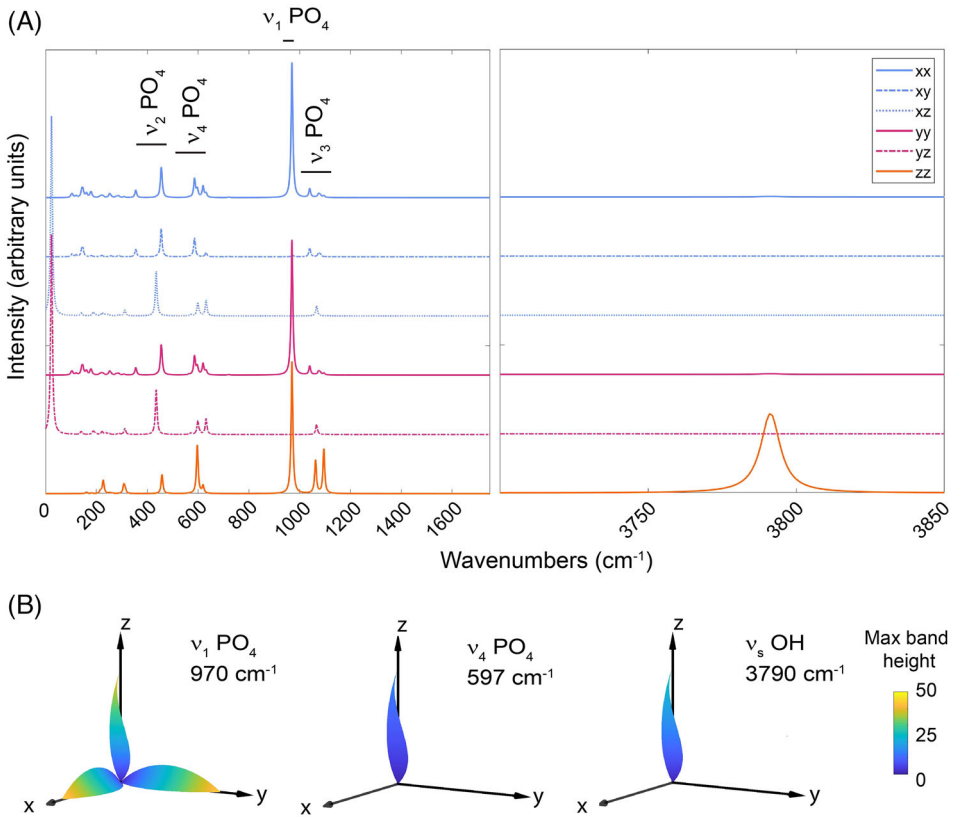

FIGURE 2 Analysis of the dependence of Raman band intensity on sample orientation of hydroxyapatite. (A) Raman spectra of hexagonal hydroxyapatite, where, for example, *xy* refers to response of the material in the *x*-direction as a result of an applied incident light source polarised in the *y*-direction. There are no bands between 1800 and 3700 cm^{-1}; therefore, this spectral range has been omitted to aid visualisation. Similarly, the spectra have been offset for clarity. (B) Three-dimensional plots showing the intensity of specific bands with respect to specific crystal-laser orientations. The intensities calculated have been linearly interpolated to predict band intensities when the laser is aligned in other orientations to those computed. Here, the axes refer to those of the crystal lattice. The colour scale reflects the highest intensity found in the spectrum, and the axes lengths are normalised to the maximum intensity of the band of interest to aid visualisation. [Colour figure can be viewed at wileyonlinelibrary.com]

which becomes more intense when the incoming light is orientated along the *z*-axis, but the crystal has an *x* or *y* orientation. Many bands important for the study of bone are even predicted to have close to zero intensity under the condition where the crystal and incoming light are orientated perpendicular to one another. For example, in the most extreme cases, such as the activity of the antisymmetric stretch of the phosphate band (ν_3 PO_4) at 1095 cm^{-1} and symmetric stretch of the OH band at 3790 cm^{-1}, the only orientation under which they are activated is when the crystal and incoming light are parallel along the *z* crystallographic axis (Figure 2B). This behaviour has been observed experimentally for the OH band, as described by Iqbal et al.[54] and Tsuda and Arends.[20] A loss of the OH band intensity upon rotation of the crystal from a parallel to 45° orientation of the laser was also found experimentally by Tsuda and Arends[20] and is confirmed by our calculations as shown in Figure 2B for this band. In Tsuda and Arends' work, the most sensitive bands to sample orientation were determined to be the antisymmetric bending ν_4 PO_4 bands around 590 cm^{-1}. In our model, the relative intensity of the 597 cm^{-1} band is largest in the *zz* orientation, whereas the intensities of neighbouring bands at 620 and 586 cm^{-1} become more dominant in other orientations. This is consistent with the observations in the literature; therefore, the DFT simulations reproduce the expected dependence of most Raman band intensities with respect to the laser orientation for hydroxyapatite crystals. However, previous experimental work has demonstrated that unlike other bands in the spectrum, the 960 cm^{-1} ν_1 PO_4 band does not exhibit the dramatic change in intensity found in the calculations.[20,54] As hexagonal fluorapatite shows an orientation dependence of this band, the lack of an orientation dependence for hydroxyapatite was explained in previous studies as evidence for a monoclinic rather than hexagonal structure.[54] In contrast, our simulations with a monoclinic structure for hydroxyapatite show the same scale of orientational behaviour as that of the hexagonal structure (Figures S1 and S2), demonstrating that differences in the lattice are not sufficient to result in the observed retention of the ν_1 PO_4 band in the Raman spectra at different orientations in single crystal experiments. Interestingly, Raman spectra of bone materials obtained at different orientations with respect to the laser polarisation do show a dependence of the ν_1 PO_4 band intensity when scattering-related errors are minimised by using a high numerical aperture lens.[14] This behaviour is most consistent with the hexagonal crystal structure as the highest intensity is found when the laser polarisation is parallel to the long axis of the bone and therefore the c-axis of the mineral. Therefore, we expect that the behaviour of this band found in the hexagonal model system is consistent with bone materials and is not related to a change in symmetry due to the presence of carbonate groups. We have thus continued to study the hexagonal form for the carbonated apatites rather than the monoclinic system based on this analysis.

3.3 | A-type carbonated apatite

To maintain charge neutrality, all OH groups in the unit cell are replaced by carbonate in our A-type carbonated apatite model. Substitution of OH by carbonate was found to produce a change in the sensitivity of the phosphate bands with respect to the polarisation of the laser. In this material, there are several ν_1 PO_4 bands with similar intensities when summed over all orientations, where the most intense are found at 959 cm^{-1} and 965 cm^{-1} (Figure 3). Overlap of these bands produced a band envelope with an apparent higher wavenumber shoulder, also observed in published work on synthetic A-type carbonate apatites.[9] Animations of these bands using CrysPlot demonstrate that the band at 965 cm^{-1} corresponds to phosphate groups located close to the carbonate, in contrast to the 959 cm^{-1} band of phosphate groups in the centre of the unit cell. Overall, these bands have a similar behaviour to that observed for the ν_1 PO_4 band in hydroxyapatite, whereby an intensity close to zero was found for configurations when the laser polarisation was perpendicular to the crystallographic axes and the highest intensity in parallel configurations. But, their behaviour with respect to orientation is slightly different. For the 959 cm^{-1} band, there was a larger change in the intensities in parallel directions where the ratios of I_{yy}:I_{xx} was 0.97 and 0.88 for I_{zz}:I_{xx}, in comparison with 1 and 0.97, respectively, in pure hydroxyapatite. In contrast, the 965 cm^{-1} band has a stronger orientation dependence producing ratios for I_{yy}:I_{xx} of 0.94 and I_{zz}:I_{xx} of 0.87, resulting in a higher prominence of this shoulder in spectrum from the *xx* configuration. The ν_4 phosphate band at 597 cm^{-1} showed only a weak direction–intensity relationship in this material.

In A-type carbonated apatite, the occupation of carbonate in the hexagonal channels within the apatite structure means that the carbonate group has a high degree of rotational freedom. Although it remains aligned with the channel length, which lies along the *z*-axis of the crystal, DFT calculations have demonstrated that there is a low energy barrier to rotation in the *xy* plane.[55] Thus, in experimental data, the carbonate signal should arise from an average of multiple orientations of carbonate within the channel. To evaluate how the orientation of the carbonate within the apatitic crystal

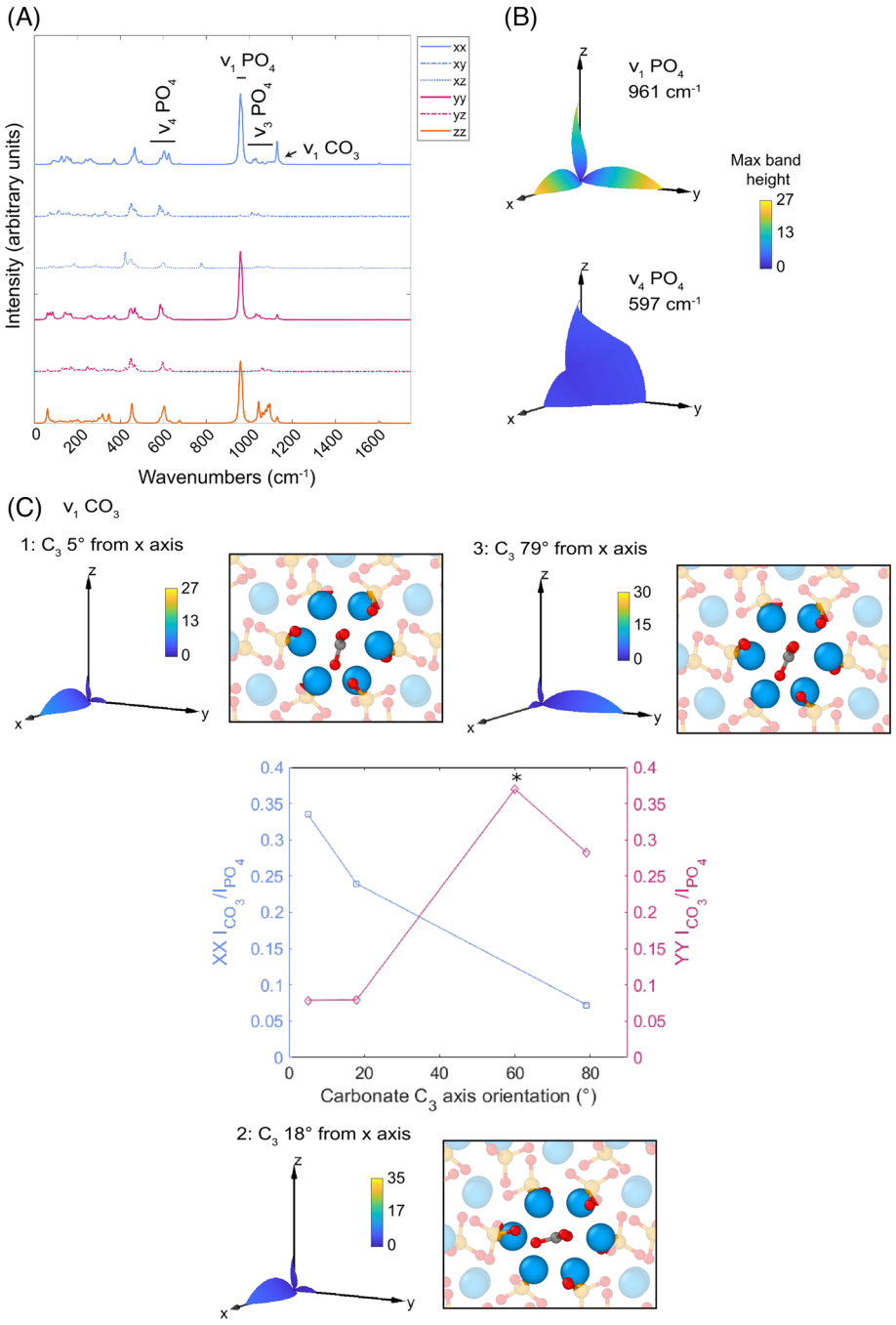

FIGURE 3 Analysis of the Raman band intensity dependence on sample orientation of A-type carbonate substituted apatite. (A) Raman spectra, where, for example, *xy* refers to response of the material in the *x*-direction as a result of an applied incident light source polarised in the *y*-direction. There are no bands above 1800 cm^{-1} as in this material, the CO_3^{2-} replaced OH^- in the structure. The spectra have been offset for clarity. (B) Three dimensional plots showing the intensity of phosphate bands with respect to specific crystal-laser orientations. (C) The effect of carbonate ion orientation in the *xy* plane on band activity. Intensity ratios of the carbonate versus the phosphate symmetrical stretch are plotted for the *xx* and *yy* configurations for models where the carbonate ion threefold rotational axis is orientated at 5°, 18°, and 79° to the *x* crystallographic axis. Due to the hexagonal unit cell, the C_3 axis is orientated along the *y* crystallographic axis at 60° in the plot. An estimate of the intensity ratio for the *yy* configuration at this point (highlighted with a *) was obtained by fitting the *xx* data with a polynomial function. Three-dimensional plots show the band intensities associated with the laser-crystal orientations for each model. Note, the plots in (a) and (B) correspond to configuration 1 in (C). For (B) and (C) 3D plots, the calculated intensities were linearly interpolated to predict band intensities when the laser is aligned in other orientations to those computed. The axis labels refer to the axes found in the crystal lattice, and the colour scale reflects the highest intensity found in the spectrum, with the axes' lengths normalised to the maximum intensity of the band of interest to aid visualisation. [Colour figure can be viewed at wileyonlinelibrary.com]

structure changes the spectra under a differently polarised laser, we analysed three stable configurations where the three-fold rotational axis (C_3) of the carbonate group is differently orientated: (1) 5°, (2) 18°, and (3) 79° from the crystallographic *x*-axis (Figure 3C). In the Raman spectra, the most active carbonate band was that associated with the symmetric carbonate stretch (ν_1). This band varied its position by 3 cm^{-1} depending on the orientation of carbonate group from 1129 cm^{-1} in configuration 3, to 1132 cm^{-1} when there was the largest misalignment from the crystallographic axes (configuration 2). This corresponds with a slight deformation of the hexagonal Ca ring in the different configurations (Figure 3B) and is up to 20 cm^{-1} higher than described previously for synthesised samples.[9] In addition to a change in position, the carbonate ν_1 band intensity had a strong dependence on the laser orientation when it was closer to the crystallographic axes, but is expected to decrease as the C_3 axis becomes unaligned (Figure 3C). Although both the carbonate and phosphate bands vary their intensity with orientation differently, the ratios of carbonate to phosphate ν_1 bands calculated for the three carbonate orientation models produced a very similar range for the *xx* and *yy* configurations, 0.07 to 0.33 and 0.08 to 0.28, respectively. By examining the different orientations, it is predicted that the maximum intensity ratios will be 0.37 when the carbonate C_3 and laser polarisation are aligned with either the *x* or *y* crystallographic axes. In contrast, there was very little variation in the carbonate to phosphate ratio (0.10 to 0.11) when the system was in the *zz* configuration, consistent with the lack of carbonate rotation with respect to this axis.

3.4 | B-type carbonated apatite

Placement of the carbonate band in the location of a phosphate group (B-type substitution) with the concomitant substitution of a Ca^{2+} for a Na^{+} to maintain charge balance results in a similar behaviour of the Raman bands to that of pristine hydroxyapatite. The lowest energy substitute configuration explored by Ulian et al.[41] was adopted for this study (labelled as the Na6 configuration model in the corresponding literature). Again, the dominant phosphate band, the symmetrical stretch (ν_1) showed the highest intensity in parallel configuration along the *xx*-axis with I_{yy}:I_{xx} and I_{zz}:I_{xx} of 0.85 and 0.90, respectively. In comparison, the ν_4 PO_4 band at 597 cm^{-1} retained its dominance in the *zz* configuration but, as observed with the A-type carbonated apatite, also has a larger intensity contribution in the other two parallel configurations, as well as the perpendicular configurations (Figure 4). Examination of the vibrations contributing to this band using CrysPlot demonstrated that unlike the unsubstituted hydroxyapatite, in the B-type carbonated apatite, the band in the spectrum is not a pristine phosphate vibration but rather is overlapped by an additional OH stretch. Therefore, some of the orientational dependency may also arise from that of the OH group. As for the A-type carbonated apatite, the carbonate group shows a strong dependency on orientation. Here, the ν_1 of carbonate in the phosphate site is found at 1091 cm^{-1}, again consistent with previous analysis of synthesised B-type carbonated apatite.[56] But this band shows a high intensity along the *zz* direction with a very low intensity in the two other parallel configurations. This information if somewhat latent and mixed in the full spectra as a result of overlapping carbonate and phosphate bands, yet it can be clearly identified from the orientational plots for specific vibrational modes (Figure 4B). Thus, for a B-type apatite, the true carbonate content would thus only be able to be measured in the parallel configuration along the *zz*, with other parallel configurations resulting in an underestimation.

3.5 | Type AB

As expected, due to the mixed nature of the AB substituted apatite structure, this material shows a combination of the behaviours found thus far for the A and B-type apatite materials with respect to sample orientation and laser polarisation. As observed for the A-type carbonate substituted apatite, the phosphate ν_1 symmetrical stretch is split into two bands, where the lower wavenumber band (967 cm^{-1} in this model) has the highest intensity in all configurations and corresponds to phosphate groups located in the centre of the unit cell (Figure 5). In contrast, the lower intensity band observed for this material at 974 cm^{-1} corresponds to phosphate located closest to A-type carbonate group substituted the equivalent position to OH in hydroxyapatite. All bands show a sensitivity to orientation, with the phosphate ν_1 symmetrical stretching modes retaining their maximum scattering efficiency when the laser is polarised parallel to a crystallographic axis, with a maximum intensity found in the *xx* configuration. Similar to the B-type apatite, the phosphate ν_4 band at 597 cm^{-1} has its maximum scattering efficiency in the *zz* configuration, but, retains its orientation dependence unlike the A-type substituted apatite.

In contrast to the A-type apatite, our simulations with different initial orientations of the carbonate group in place of an OH group (A-type carbonate substitution) in the AB-type model reverted to the lowest energy state described previously by Ulian et al.[41] In other words,

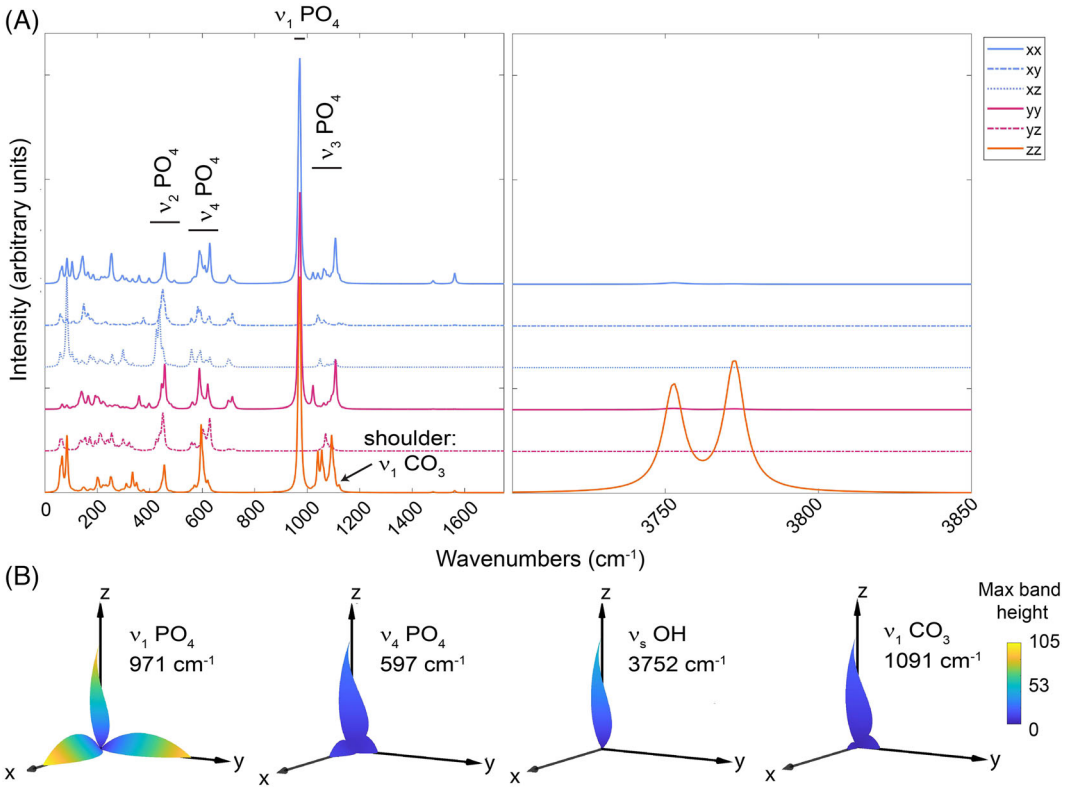

FIGURE 4 Raman spectra and intensities of specific bands with respect to the orientation between the laser and crystal structure for the B-substituted hydroxyapatite, where carbonate substitutes for a phosphate group within the apatite structure. (A) Raman spectra of different orientations between the incoming laser light and crystal structure. Here, for example, *yz* refers to the response of B-substituted hydroxyapatite orientated in the *y*-direction as a result of an applied incident light source polarised in the *z*-direction. There are no Raman bands determinable from the simulations between 1800 cm^{-1} and 3700 cm^{-1}; therefore, this spectral region has been omitted. The individual spectra have been offset to aid visualisation. (B) Plots showing the three-dimensional relationship between crystal orientation and laser polarisation. Intensities obtained from the simulations were linearly interpolated to predict band intensities when the laser is polarised in other orientations to those computed. Here, the axes refer to the axes in the crystal lattice. The axes' lengths are normalised to the maximum intensity of the band of interest whereas the colour scale reflects the highest intensity found in the spectrum. [Colour figure can be viewed at wileyonlinelibrary.com]

the rotational energy barrier for carbonate in the hexagonal channel that runs along the *z*-axis seems to be much higher in the AB-type carbonated apatite. This is likely due to the replacement of a Ca^{2+} ion at the edge of the channel with an Na^{+} ion (Figure 1), required to maintain charge balance when a phosphate group is replaced by carbonate (B-type carbonate substitution). The carbonate C_3 axis in the AB-type structure is positioned 78° from the *x*-axis in the AB-type model, which is almost identical to configuration 3 in the A-type carbonated apatite model. However, the orientation sensitivity of the carbonate ν_1 band and its intensity were much lower as the *xx* and *yy* carbonate to phosphate ν_1 band ratios were 0.009 and 0.005 for the AB-type system, respectively, whereas they were 0.07 and 0.28 for the A-type model, respectively. A maximum scattering efficiency for the carbonate ν_1 band was found in the *zz* configuration for the AB-type carbonate substituted apatite, with $I_{xx:zz}$ and $I_{yy:zz}$ of 0.51 and 0.24, whereas the maximum difference in the perpendicular directions (in the *xz* configuration) is also 0.24 with respect to the *zz* scattering efficiency, with other directions producing an intensity even lower. The ν_1 symmetrical stretch of carbonate in the B-site of the AB substituted structure was found at the same location as the equivalent band in the B-type carbonate substituted apatite. However, the presence of the A-type carbonate appears to result in a change in the behaviour of the bands related to the carbonate substituted for phosphate. For example, the ν_1 symmetrical stretch of carbonate in the B-site found at 1091 cm^{-1} showed the same scattering efficiency in both the *xx* configuration and *yy* configuration as well as an intensity ratio for $I_{zz:xx}$ of 0.57, whereas in a perpendicular configuration, the highest intensity ratio was 0.10. Despite showing a similar behaviour with respect to the activity of bands in different configurations, the changes in scattering efficiency are not the same for the phosphate and carbonate related bands. In the parallel configurations, where the intensity is

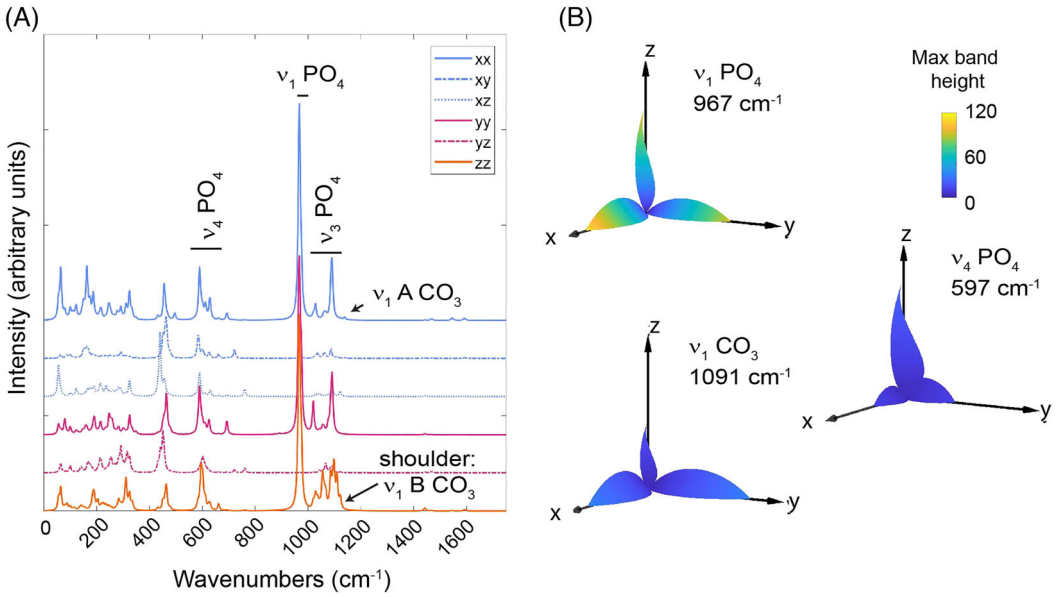

FIGURE 5 Raman spectra and intensities of specific bands with respect to the orientation between the laser and crystal structure for the AB-substituted hydroxyapatite, where carbonate substitutes in both an A- and B-sites within the apatite structure. (A) Raman spectra of different orientations between the incoming laser light and crystal structure. Here, for example, *yz* refers to the response of AB-substituted hydroxyapatite orientated in the *y*-direction as a result of an applied incident light source polarised in the *z*-direction. Individual spectra have been offset to aid visualisation and comparison. (B) Plots showing the three dimensional relationship between crystal orientation and laser polarisation. Intensities obtained from the simulations were linearly interpolated to predict band intensities when the laser is polarised in other orientations to those computed. Here, the axes refer to the axes in the crystal lattice. The axes' lengths are normalised to the maximum intensity of the band of interest whereas the colour scale reflects the highest intensity found in the spectrum. [Colour figure can be viewed at wileyonlinelibrary.com]

highest, the difference in scattering efficiency would result in a CO_3:PO_4 ratio of 0.29, 0.35 and 0.18 for *xx*, *yy*, and *zz*, respectively.

4 | IMPLICATIONS FOR BONE ANALYSIS

Orientation of crystallites within bone is an important component of bone's mechanical function,[57] including during its regeneration.[8] It is known that the bioapatite crystals within bone can be orientated with respect to the collagen fibrils and thus the lamellae that are present at a higher level of the hierarchical arrangement in bone.[58] The absolute orientation of the bioapatite with respect to the bone characteristics will therefore be dependent on the type of bone, as compact bone in long bones has a different organisation at higher levels of the hierarchical material than spongy cancellous bone.[59,60] Even in woven bone, where there is no measurable fibril orientation, bone mineral crystallites are observed to become orientated with time.[61] However, within a single compact bone, there can be different amounts of organisation, for example, two mineralised fibre arrangements are present, twisted, or orthogonal plywood structure, where differences in the relative intensities of Raman bands have been used to evaluate their presence.[62] Similarly, in rats, the level of organisation was not found to be consistent across a single bone specimen.[63] In addition, the organisation of the bone structure and therefore the alignment of the bone mineral component can vary with age,[13] up to puberty in humans,[64] and in cases where a bone mineralisation disease is present.[65]

The observation that orientation would be expected to play a significant role in characterising bone materials is reflected in Raman spectroscopic analysis of these materials where the ν_1 PO_4 band intensity was found to depend on the orientation of the mineral with respect to the polarisation of the laser.[14] However, while it is an acceptable method to use Raman spectroscopy to evaluate the carbonate:phosphate ratios within bone,[66] the effect of orientation on this data is typically neglected in these analyses. The calculations conducted here clearly show that apatite phosphate band intensities are orientationally dependent. This not only applies to hydroxyapatite but also is consistent with our models of carbonated apatite, supporting the use of phosphate bands for Raman spectroscopy-based orientational studies as described in the literature. However, the carbonate bands are also highly orientation dependent and are not expected to scale directly with the intensity changes of the phosphate band based on the simulations. Even

Raman instruments without the ability to polarise the laser along different directions can produce orientation effects in mineral spectra.[67] Therefore, this effect is expected to be present in mineral characteristic studies as well.

In compact bone, it has been reported that 75% of the crystallites lie outside of the collagen matrix and that these crystals are highly aligned with their c-axis lying parallel to the long axis of the bone.[68] Evaluation of the effect of orientation within the crystal on the measured ratios indicates a variability in the ratios of up to 23% for the B- and 17% AB-type carbonated apatite. Based on the calibrated lines of synthetic B-carbonated apatite,[69] this would be a variation in the carbonate content of 10 weight %. Given that the largest discrepancies for both the B and AB-type carbonated apatites are between the *zz* and *xx* or *yy* orientations, this implies that limiting the difference in orientation through analysing perpendicular to the long axis of the bone or collagen alignment should produce the most robust carbonate data, although they will reflect an underestimation in the carbonate content. When examining the difference between the *xx* and *yy* orientations, the difference in the carbonate:phosphate ratios are much lower, 6% for both B- and AB-type carbonated apatite, resulting in a difference of 1 weight % carbonate when using the synthetic calibration lines. A previous study exploring longitudinally cross-sectioned compact bone found higher carbonate contents of several weight % related to less crystallite alignment in bone associated with a mineralisation disorder. In contrast, in the same study, a decrease in carbonate with increasing alignment was found related to age in normal mice.[70] This indicates that decreasing alignment of the crystallites does not scale directly with increasing carbonate content, which would be expected if an increased *zz* component was significant during the analysis of less organised bone. Thus, increased carbonate content related to bone mineralisation diseases was not the consequence of changes in the bone organisation. The variability of organisation within the bone structure requires that specific areas, such as close to osteons, should be avoided and many points taken to make a statistically robust measurement that can account for more variations. In addition, our findings suggest that there may be a population of the bone crystals in the randomly organised crystals that are not being effectively mapped by the Raman spectrometer during analysis if they are orientated perpendicular to the laser polarisation.

Interestingly, B-type carbonated apatites have been reported to have a lower OH band intensity with increasing carbonate substitution,[71] consistent with the observation of a lack of OH within the crystal structure in bone crystallites.[24] Our simulations demonstrate that for a structure that has 17% carbonate content, that is, one out of six phosphate sites it taken up by a carbonate ion, which is higher than the typical content reported for synthesised samples, the OH band should remain Raman active.

In the B-type carbonated apatite, the OH band becomes split due to the lowering of symmetry in the simulations from $P6_3$ in hydroxyapatite to $P1$. Yet, the OH/ν_1 PO_4 intensity ratio was very similar (0.61) for the most intense OH band of the B-type carbonate hydroxyapatite compared with that found in the hydroxyapatite (0.60). Therefore, if OH was present in bone bioapatite and the sample was randomly orientate or along *zz*, the simulations indicate OH stretching bands should be visible in the Raman spectrum. Its absence in previous work[24] that studied an extracted powder that is assumed to be randomly orientated, thus, supports the hypothesis that bone bioapatite does not contain significant amounts of OH consistent with later NMR analyses.[72]

A range of positions for the B-type carbonate ν_1 band have been reported from 1072 to 1080 cm^{-1} depending on the phase composition, including the presence of other substitute ions such as silica, and crystallinity.[73] Most synthetic materials of the A- or B-carbonated apatite report ν_1 carbonate bands that are $\sim$30 cm^{-1} apart, consistent with previous simulations of different AB-carbonate structures with the exception of one model where the ν_1 band positions of A-type carbonate were found to be lower than the equivalent B-type band.[41] A later paper has demonstrated that the exact spacing of these bands changed depending on pressure.[74] Therefore, there is a chance that there may be some overlap between A- and B-type ν_1 carbonate bands depending on the sample chemistry. Critically, even if the bands are distinguishable, our model demonstrates that the activity of the A-type band is expected to be lower in the AB-type carbonated apatite system. Thus, it is possible that in bone and synthesised carbonated apatite, some carbonate also substitutes for the OH but is not detectable using Raman spectroscopy. This would be consistent with IR spectroscopy analysis of bone, which detects carbonate in the A-type site.[75]

5 | CONCLUSION

Density functional theory calculations of hydroxyapatite and carbonated apatite structures have demonstrated a consistency with experimentally derived systems reported in the literature, including their response to orientation where this information is available. It became clear from the simulations that the apatite system has a strong orientation dependency of the Raman band intensities and

that these behaviours differ depending on the band examined. This means that ratios of critical bands, such as the ν_1 of phosphate and carbonate, are not consistent between different orientations. In particular, the *zz* orientations have the highest sensitivity to both phosphate and carbonate and produce the largest ratio value. In comparison, there is almost no intensity observed for the phosphate and carbonate bands in orientations where the laser is aligned perpendicular to the crystallographic axes of the apatites studied. This means that for orientation studies, evaluations of bone cut perpendicular to the collagen structure will produce the most sensitive information. However, samples cut parallel to the collagen structure will be most effective for examining changes in carbonate content between specimens as the ratios of the carbonate and phosphate band intensities are most robust in this orientation because they are not as affected by orientation of the crystallites.

ACKNOWLEDGEMENTS

The work has been performed under the Project HPC-EUROPA3 (INFRAIA-2016-1-730897), with the support of the EC Research Innovation Action under the H2020 Programme; in particular, the author gratefully acknowledges the support of Department of Earth Sciences, Utrecht University, Netherlands, and the computer resources and technical support provided by SURFsara.

ORCID

Aleksandar Živković https://orcid.org/0000-0003-1347-6203
Igor Lukačević https://orcid.org/0000-0002-7277-5089

REFERENCES

[1] T. Kono, T. Sakae, H. Nakada, T. Kaneda, H. Okada, *Minerals* **2022**, *12*, 170.
[2] F. Ren, Y. Ding, Y. Leng, *J. Biomed. Mater. Res. Part A* **2014**, *102*, 496.
[3] A. A. Baig, J. L. Fox, J. Hsu, Z. Wang, M. Otsuka, W. I. Higuchi, R. Z. LeGeros, *J. Colloid Interface Sci.* **1996**, *179*, 608.
[4] J.-D. P. McElderry, P. Zhu, K. H. Mroue, J. Xu, B. Pavan, M. Fang, G. Zhao, E. McNerny, D. H. Kohn, R. T. Franceschi, M. M. B. Holl, M. M. J. Tecklenburg, A. Ramamoorthy, M. D. Morris, *J. Solid State Chem.* **2013**, *206*, 192.
[5] S. Bertazzo, E. Gentleman, K. L. Cloyd, A. H. Chester, M. H. Yacoub, M. M. Stevens, *Nat. Mater.* **2013**, *12*, 576.
[6] A. Boskey, R. Mendelsohn, *J. Biomed. Opt.* **2005**, *10*, 031102.
[7] B. Wan, R. Wang, Y. Sun, J. Cao, H. Wang, J. Guo, D. Chen, *Front. Bioeng. Biotechnol.* **2020**, *8*, 1176.
[8] T. Ishimoto, T. Nakano, Y. Umakoshi, M. Yamamoto, Y. Tabata, *J. Bone Miner. Res.* **2013**, *28*, 1170.
[9] G. Penel, G. Leroy, C. Rey, E. Bres, *Calcif. Tissue Int.* **1998**, *63*, 475.
[10] B. Wopenka, J. D. Pasteris, *Mater. Sci. Eng. C* **2005**, *25*, 131.
[11] M. Kazanci, H. D. Wagner, N. I. Manjubala, H. S. Gupta, E. Paschalis, P. Roschger, P. Fratzl, *Bone* **2007**, *41*, 456.
[12] J. S. Nyman, A. J. Makowski, C. A. Patil, T. P. Masui, E. C. O'Quinn, X. Bi, S. A. Guelcher, D. P. Nicollela, A. Mahadevan-Jansen, *Calcif. Tissue Int.* **2011**, *89*, 111.
[13] S. Gamsjaeger, A. Masic, P. Roschger, M. Kazanci, J. W. C. Dunlop, K. Klaushofer, E. P. Paschalis, P. Fratzl, *Bone* **2010**, *47*, 392.
[14] M. Raghavan, N. D. Sahar, R. H. Wilson, M.-A. Mycek, N. Pleshko, D. H. Kohn, M. D. Morris, *J. Biomed. Opt.* **2010**, *15*, 037001.
[15] E. A. Taylor, C. J. Mileti, S. Ganesan, J. H. Kim, E. Donnelly, *Calcif. Tissue Int.* **2021**, *109*, 77.
[16] F. Esmonde-White, M. Morris, in *Progress in Biomedical Optics and Imaging - Proceedings of SPIE*, **2013**, *8565*, p. 85656K.
[17] P. Matousek, E. R. C. Draper, A. E. Goodship, I. P. Clark, K. L. Ronayne, A. W. Parker, *Appl. Spectrosc.* **2006**, *60*, 758.
[18] K. Buckley, J. G. Kerns, P. D. Gikas, H. L. Birch, J. Vinton, R. Keen, A. W. Parker, P. Matousek, A. E. Goodship, *IBMS BoneKey* **2014**, *11*, 602.
[19] G. Leroy, G. Penel, N. Leroy, E. Brès, *Appl. Spectrosc.* **2002**, *56*, 1030.
[20] H. Tsuda, J. Arends, *J. Dent. Res.* **1994**, *73*, 1703.
[21] M. Georgiadis, R. Müller, P. Schneider, *J. R. Soc. Interface* **2016**, *13*, 20160088.
[22] C. D. Lopes, P. H. J. O. Limirio, V. R. Novais, P. Dechichi, *Appl. Spectrosc. Rev.* **2018**, *53*, 747.
[23] G. Daculsi, J. Menanteau, L. M. Kerebel, D. Mitre, *Calcif. Tissue Int.* **1984**, *36*, 550.
[24] J. D. Pasteris, B. Wopenka, J. J. Freeman, K. Rogers, E. Valsami-Jones, J. A. M. van der Houwen, M. J. Silva, *Biomaterials* **2004**, *25*, 229.
[25] R. Dovesi, V. R. Saunders, C. Roetti, R. Orlando, C. M. Zicovich-Wilson, F. Pascale, B. Civalleri, K. Doll, N. M. Harrison, I. J. Bush, P. D'Arco, M. Llunell, M. Causà, Y. Noël, L. Maschio, A. Erba, M. Rerat, S. Casassa, University of Torino, Torino **2017**.
[26] R. Dovesi, A. Erba, R. Orlando, C. M. Zicovich-Wilson, B. Civalleri, L. Maschio, M. Rérat, S. Casassa, J. Baima, S. Salustro, B. Kirtman, *WIREs Comput. Mol. Sci.* **2018**, *8*, 1.
[27] L. Valenzano, F. J. Torres, K. Doll, F. Pascale, C. M. Zicovich-Wilson, R. Dovesi, *Zeitschrift fur Phys. Chemie* **2006**, *220*, 893.
[28] C. M. Zicovich-Wilson, A. Bert, C. Roetti, R. Dovesi, V. R. Saunders, *J. Chem. Phys.* **2002**, *116*, 1120.
[29] M. Corno, C. Busco, B. Civalleri, P. Ugliengo, *Phys. Chem. Chem. Phys.* **2006**, *8*, 2464.
[30] C. Gatti, V. R. Saunders, C. Roetti, *J. Chem. Phys.* **1994**, *101*, 10686.
[31] M. Catti, A. Pavese, R. Dovesi, V. R. Saunders, *Phys. Rev. B* **1993**, *47*, 9189.
[32] R. Dovesi, C. Roetti, C. Freyria-Fava, M. Prencipe, V. R. Saunders, *Chem. Phys.* **1991**, *156*, 11.
[33] A. D. Becke, *J. Chem. Phys.* **1993**, *98*, 1372.
[34] C. Lee, W. Yang, R. G. Parr, *Phys. Rev. B* **1988**, *37*, 785.
[35] R. Dovesi, V. R. Saunders, C. Roetti, R. Orlando, F. Pascale, B. Civalleri, K. Doll, N. M. Harrison, I. J. Bush, P. D. Arco, M. Llunel, M. Caus, *J. Chem. Phys.* **2013**, *139*, 167101. https://doi.org/10.1063/1.4826136

[36] R. Dovesi, B. Kirtman, L. Maschio, J. Maul, F. Pascale, M. Rérat, *J. Phys. Chem. C* **2019**, *123*, 8336.
[37] L. Maschio, B. Kirtman, M. Rérat, R. Orlando, R. Dovesi, *J. Chem. Phys.* **2013**, *139*, 167101.
[38] M. Corno, C. Busco, V. Bolis, S. Tosoni, P. Ugliengo, *Langmuir* **2009**, *25*, 2188.
[39] G. Ulian, G. Valdrè, *J. Mech. Behav. Biomed. Mater.* **2018**, *77*, 683.
[40] G. Ulian, G. Valdre, M. Corno, P. Ugliengo, *Am. Mineral.* **2013**, *98*, 410.
[41] G. Ulian, G. Valdre, M. Corno, P. Ugliengo, *Am. Mineral.* **2014**, *99*, 117.
[42] F. Pascale, S. Tosoni, C. Zicovich-Wilson, P. Ugliengo, R. Orlando, R. Dovesi, *Chem. Phys. Lett.* **2004**, *396*, 308.
[43] P. Ugliengo, F. Pascale, M. Mérawa, P. Labéguerie, S. Tosoni, R. Dovesi, *J. Phys. Chem. B* **2004**, *108*, 13632.
[44] S. Grimme, S. Ehrlich, L. Goerigk, *J. Comput. Chem.* **2011**, *32*, 1456.
[45] S. Grimme, A. Hansen, J. G. Brandenburg, C. Bannwarth, *Chem. Rev.* **2016**, *116*, 5105.
[46] S. Grimme, J. Antony, S. Ehrlich, H. Krieg, *J. Chem. Phys.* **2010**, *132*, 154104.
[47] K. Momma, F. Izumi, *J. Appl. Cryst.* **2011**, *44*, 1272.
[48] V. Wang, N. Xu, J. C. Liu, G. Tang, W.-T. Geng, **2019**, *1*.
[49] S. S. Bhat, U. V. Waghmare, U. Ramamurty, *Cryst. Growth Des.* **2014**, *14*, 3131.
[50] F. Ren, X. Lu, Y. Leng, *J. Mech. Behav. Biomed. Mater.* **2013**, *26*, 59.
[51] D. Aquilano, M. Bruno, M. Rubbo, F. R. Massaro, L. Pastero, *Cryst. Growth Des.* **2014**, *14*, 2846.
[52] B. Civalleri, C. M. Zicovich-Wilson, L. Valenzano, P. Ugliengo, *CrstEngComm* **2008**, *10*, 405.
[53] G. Ulian, G. Valdré, M. Corno, P. Ugliengo, *Am. Mineral.* **2013**, *98*, 752.
[54] Z. Iqbal, V. P. Tomaselli, O. Fahrenfeld, K. D. Möller, F. A. Ruszala, E. Kostiner, *J. Phys. Chem. Solid* **1977**, *38*, 923.
[55] F. Peccati, M. Corno, M. Delle Piane, G. Ulian, P. Ugliengo, G. Valdrè, *J. Phys. Chem. C* **2014**, *118*, 1364.
[56] K. Benataya, M. Lakrat, L. L. Elansari, E. Mejdoubi, *Mater. Today Proc.* **2020**, *31*, 83.
[57] M. Granke, A. Gourrier, F. Rupin, K. Raum, F. Peyrin, M. Burghammer, A. Saïed, P. Laugier, *PLoS ONE* **2013**, *8*, e58043.
[58] D. Jaschouz, O. Paris, P. Roschger, H.-S. Hwang, P. Fratzl, *J. Appl. Cryst.* **2003**, *36*, 494.
[59] N. Sasaki, N. Matsushima, T. Ikawa, H. Yamamura, A. Fukuda, *J. Biomech.* **1989**, *22*, 157.
[60] M. Kazanci, P. Roschger, E. P. Paschalis, K. Klaushofer, P. Fratzl, *J. Struct. Biol.* **2006**, *156*, 489.
[61] Y. Takano, C. H. Turner, D. B. Burr, *J. Bone Miner. Res.* **1996**, *11*, 1292.
[62] G. Falgayrac, S. Facq, G. Leroy, B. Cortet, G. Penel, *Appl. Spectrosc.* **2010**, *64*, 775.
[63] M. J. Turunen, J. D. Kaspersen, U. Olsson, M. Guizar-Sicairos, M. Bech, F. Schaff, M. Tägil, J. S. Jurvelin, H. Isaksson, *J. Struct. Biol.* **2016**, *195*, 337.
[64] S. Chatterji, J. C. Wall, J. W. Jeffery, *Calcif. Tissue Int.* **1981**, *33*, 567.
[65] W. Tesch, T. Vandenbos, P. Roschgr, N. Fratzl-Zelman, K. Klaushofer, W. Beertsen, P. Fratzl, *J. Bone Miner. Res.* **2003**, *18*, 117.
[66] M. D. Morris, G. S. Mandair, *Clin. Orthop. Relat. Res.* **2011**, *469*, 2160.
[67] H. E. King, D. C. Mattner, O. Plümper, T. Geisler, A. Putnis, *Cryst. Growth Des.* **2014**, *14*, 3910.
[68] R. M. V. Pidaparti, A. Chandran, Y. Takano, C. H. Turner, *J. Biomech.* **1996**, *29*, 909.
[69] A. Awonusi, M. D. Morris, M. M. J. Tecklenburg, *Calcif. Tissue Int.* **2007**, *81*, 46.
[70] H. E. King, S. M. Tommasini, A. B. Rodriguez-Navarro, B. Q. Mercado, H. C. W. Skinner, *J. Appl. Cryst.* **2019**, *52*, 960.
[71] M. Wang, R. Qian, M. Bao, C. Gu, P. Zhu, *Mater. Lett.* **2018**, *210*, 203.
[72] G. Cho, Y. Wu, J. L. Ackerman, *Science* **2003**, *300*, 1123.
[73] A. Antonakos, E. Liarokapis, T. Leventouri, *Biomaterials* **2007**, *28*, 3043.
[74] G. Ulian, D. Moro, G. Valdrè, *Am. Mineral.* **2021**, *106*, 1928.
[75] C. Rey, B. Collins, T. Goehl, I. R. Dickson, M. J. Glimcher, *Calcif. Tissue Int.* **1989**, *45*, 157.

SUPPORTING INFORMATION

Additional supporting information can be found online in the Supporting Information section at the end of this article.

How to cite this article: D. Gemeri, A. Živković, I. Lukačević, H. Bahmann, H. E. King, *J Raman Spectrosc* **2023**, *54*(2), 159. https://doi.org/10.1002/jrs.6465